34th Annual International Conference of the IEEE EMBS
San Diego, California USA, 28 August - 1 September, 2012

Anterior Chamber Angle Classification Using Multiscale Histograms of Oriented Gradients for Glaucoma Subtype Identification*

Yanwu Xu[1], Jiang Liu[1], Ngan Meng Tan[1], Beng Hai Lee[1], Damon Wing Kee Wong[1], Mani Baskaran[2], Shamira A. Perera[2] and Tin Aung[2,3]

Abstract— **Glaucoma subtype can be identified according to the configuration of the anterior chamber angle(ACA). In this paper, we present an ACA classification approach based on histograms of oriented gradients at multiple scales. In digital optical coherence tomography (OCT) photographs, our method automatically localizes the ACA, and extracts histograms of oriented gradients (HOG) features from this region to classify the angle as an open angle (OA) or an angle-closure(AC). This proposed method has three major features that differs from existing methods. First, the ACA localization from OCT images is fully automated and efficient for different ACA configurations. Second, the ACA is directly classified as OA/AC by using multiscale HOG visual features only, which is different from previous ACA assessment approaches that on clinical features. Third, it demonstrates that visual features with higher dimensions outperform low dimensional clinical features in terms of angle closure classification accuracy. Testing was performed on a large clinical dataset, comprising of 2048 images. The proposed method achieves a 0.835 ± 0.068 AUC value and $75.8\% \pm 6.4\%$ balanced accuracy at a 85% specificity, which outperforms existing ACA classification approaches based on clinical features.**

I. Introduction

Glaucoma is the second leading cause of blindness worldwide (behind cataracts) as well as the foremost cause of irreversible blindness [1], with a mean prevalence of 2.4% for all age groups and 4.7% for ages 75 years and above. It currently affects about 60 million people [2], and is responsible for approximately 5.2 million cases of blindness (15% of world total) according to the data from the World Health Organization [1]. As illustrated in Fig. 1, *glaucoma is classified according to the configuration of the angle* (formed by the intersection of the cornea and iris) into open angle (OA) and angle-closure (AC) glaucoma. Primary angle closure glaucoma (PACG) is a major form of glaucoma in Asia [3], compared to primary open angle glaucoma (POAG), which is more common in Caucasians and Africans [4]. The high visual morbidity from PACG is related to the destructive nature of the asymptomatic form of the disease.

*This work was supported in part by the Agency for Science, Technology and Research, Singapore, under BMRC grant 10/1/35/19/674.

[1]Y.-W. Xu, J. Liu, N.-M. Tan, B.-H. Lee and D.W.K. Wong are with the Institute for Infocomm Research, Agency for Science, Technology and Research, 138632, Singapore {yaxu, jliu, nmtan, benghai, wkwong} at i2r.a-star.edu.sg

[2]M. Baskaran, S.A. Perera and T. Aung are with the Singapore Eye Research Institute, 168751, Singapore baskaran.mani at seri.com.sg, shamira.perera at snec.com.sg, aung.tin at snec.com.sg

[3]T. Aung is also with the Department of Ophthalmology, National University of Singapore, 119074, Singapore

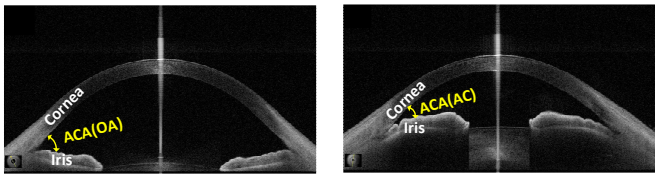

Fig. 1. Open angle (OA, left) and angle-closure (AC, right).

Early detection of anatomically narrow angles is important and the subsequent prevention of visual loss from PACG depends on an accurate classification of the ACA [5].

Angle closure is a result of obstruction of the trabecular meshwork by the iris, impeding the drainage of aqueous humour in the angle of the eye, causing an increase in intraocular pressure (IOP). As reported in [6], a shallow central anterior chamber depth (ACD), a thick and anterior lens position and short axial length (AL) are anatomical risk factors for angle closure. Amongst these, a shallow ACD is regarded as a cardinal risk factor for PACG. However, only a small proportion of subjects with shallow ACD ultimately develop PACG according to a population study [7]. Thus other ocular factors related to PACG development need to be discovered.

In the literature, automated glaucoma subtype classification has been studied on color RetCam images [8], in which the biologically inspired features (BIF) are extracted from the ACA regions for classification. For other image modalities, several automatic ACA assessment methods have been proposed. For example, an edge detection and line fitting approach is proposed for ACA measurement [9] in ultrasound biomicroscopy (UBM) images. Similarly, a segmentation, edge detection and linear regression based approach is proposed for ACA assessment in OCT images [10].

In this work, we study ACA classification based on histograms of oriented gradients (HOG) features to identify glaucoma subtype in OCT images, which has the advantages of being non-invasive and non-contact [11] compared to UBM. An OCT image captures a cross-section of the eye as a grayscale image, and several features can be extracted for ACA measurement, such as anterior chamber open depth (AOD) [9][10], trabeculariris angle (TIA) [12], trabecular-iris space area (TISA) [12] and Schwalbe's line bounded area (SLBA) [13]. *In clinical practice, these features are used for ACA classification.*

978-1-4577-1787-1/12/$26.00 ©2012 IEEE

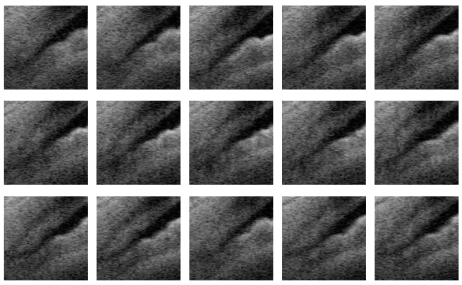

Fig. 2. Illustration of the varying of ACA closed and open. The ACAs in the top and bottom rows are clinically labeled as closed, the ACAs in middle row are labeled as open; however, these ACAs are intermediate cases and very hard to classify.

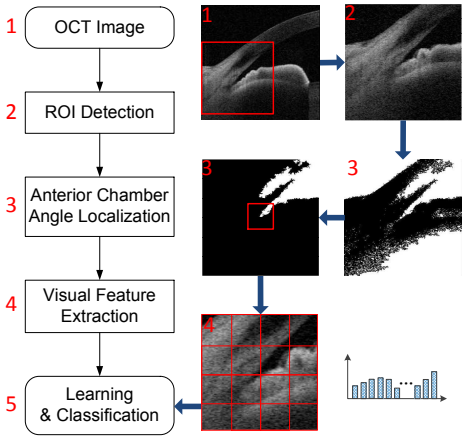

Fig. 3. Flowchart of the proposed ACA localization and classification.

ACA detection in OCT images can be relatively straightforward since the images are generally clean and are approximately aligned during image acquisition process. However, ACA classification is a challenging task since there are intermediate cases (see in Fig. 2) that are difficult to classify as AC or OA using the same clinical features, even for human experts. Based on image classification experience, using only one or two dimensional clinical features is insufficient to achieve good performance, since the eigen dimension of this problem might be much higher, *as observed clinically* [7].

In this paper, we propose an image processing and learning based framework for efficient ACA localization and classification, which has the following main features: 1) the image processing based ACA localization in OCT images is fully automated and efficient for different ACA configurations; 2) it can directly classify ACA as OA/AC based on only visual features, which is different from previous work for ACA measurement that relies on clinical features; 3) it demonstrates that visual features with higher dimensions outperform low dimensional clinical features in terms of angle closure classification accuracy. With the proposed framework, other existing visual features and learning algorithms can be introduced to elevate performance.

II. ACA Localization and Classification Framework

To classify an ACA as open or closed angles, our solution is to follow the method of a human expert. As shown in Fig. 3, for a given OCT image, we first localize the ACA region by using image processing approaches, and then extract certain visual features (*e.g., HOG*) in the region and apply the SVM classifier to identify whether it is closed. In previous work, the ACA regions are marked manually [12] or are automatic determined by using edge detection [9]. Based on our observations, we extended the edge detection approach by combining edge detection with weighting and connected component labeling segmentation (CCLS) [10], which is robust to different ACA configurations and can localize the ACAs with their vertices roughly aligned. To classify an ACA as AC or OA, the simple thresholding method is clinically used with several clinical features (*e.g.*, depth, angle and area) for ACA measurement. However, we believe that the context around the ACA region can provide additional information to increase classification accuracy, since the eigen dimension of this problem might be much higher. Thus we introduce HOG features at multiple scales with higher dimension and SVM classifier for ACA classification.

A. ACA localization

A coarse-to-fine scheme is used to efficiently localize the ACA from input OCT image. As shown in Fig. 3, first, a 400×400 region of interest (ROI) covering the exact ACA is cropped out at a fixed position from the 834×900 input image; second, the ROI is quantized to a binary image (0 for black and 1 for white) using a small valued threshold in order to preserve more details of the angle (a large/adaptive threshold will lose more details at the extreme end of the ACA, which is very important for classification); third, a morphological operation is performed to remove isolated noise points; fourth, weighting and CCLS algorithm are used to segment the ACA candidate in the ROI; fifth, a post processing step is applied to remove other components connected to the exact ACA in the candidate region; lastly, the ACA is localized with an $n \times n$ bounding box centered at its detected vertex.

1) ROI detection: For ROI detection, many existing computer vision methods can be used, such as the well-known sliding window method [14][15]. However, for the relatively clean OCT images, line fitting based cornea detection is accurate and much more efficient to obtain the ROI, since the ACA is between the cornea and iris (see in Fig. 1). As shown in Fig. 4, Sobel edge detection is first applied on the OCT image, and then the top-most white point of each column is obtained, thus the fitted smooth line of these points is treated as the upper boundary of the cornea. The lowest point of the boundary is selected as the reference point (*i.e.*, the center point of the left boundary of the ROI), and then a 400×400 rectangle referred to this point is cropped as the ROI.

2) ACA segmentation: The ROI is first converted to binary image (0 for black and 1 for white) using a small valued

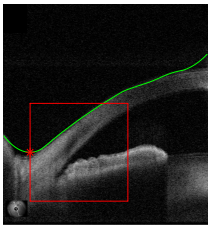

Fig. 4. Illustration of ROI detection. The green line is the detected cornea upper boundary and the red bounding box is the ROI.

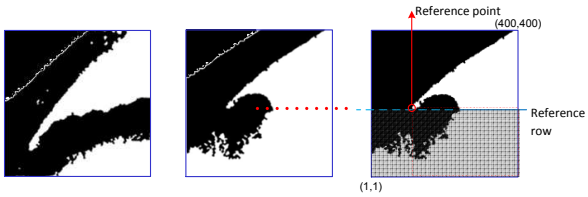

Fig. 5. Clear ACA (left), bottom connected ACA (middle) and an illustration of post processing (right) for the bottom connected case.

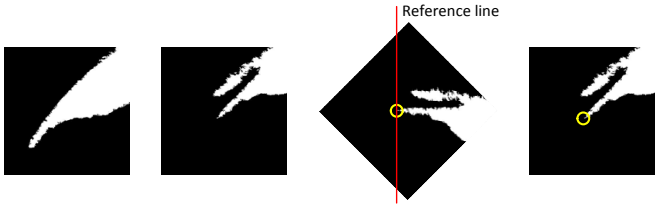

Fig. 6. Two ACA profiles: single clear angle (first) and multiple angles (second), and illustration of ACA vertex localization (third and fourth) for an ACA region.

threshold, and the pixels above the cornea upper boundary is set to black to avoid further processing. Thus each 4-connected white region can be separated and labeled by using CCLS algorithm [10], and the candidate ACA region is selected by choosing the one with maximum pixel number. With the candidate ACA region obtained, a post processing step illustrated in Fig. 5 is applied to deal with the case that the bottom part of the ACA is connected with other white regions. This occurs when *the iris is not fully captured during the imaging process*, resulting in that at least one row is completely white in the bottom half of the right-most rows. First, the top-most white point of each column is located; second, the difference between each pair of neighboring columns is computed; third, the first column from the left that has a difference greater than 30 (pixels) is found and then the reference point of the ACA segmentation can be obtained; lastly, for the region from the reference point to the right-bottom, a zero value (black) is given to all the pixels below the reference row which has the minimum number of white pixels.

3) ACA vertex localization: As shown in Fig. 6, by this step, the obtained ACA regions can be categorized into two profiles according to our observations, *i.e.*, the clear case (when the ACA vertex is the left-bottom-most white point) and the multiple angles case. To localize the true vertex of the ACA in both cases, the image is first rotated 45 degree clockwise with respect to the bottom-left point, and then the left-most white point is located (if there are multiple such points, choose the bottom-most one) and its original position on the non-rotated image can be calculated. After the vertex is localized, a $n \times n$ (n is set to 150 in the experiments) region centered at the vertex is cropped *from the original image*, as the ACA localization result to extract visual features for classification.

B. ACA feature representation and classification

1) HOG feature extraction: In this work, HOG features [14] is used for ACA representation, because HOG features have demonstrated great success in various object detection and recognition problems. Moreover, HOG features are related to the edge information, which is important for ACA assessment; and we did not use BIF features [8] which are related to textures, computational expensive and are more suitable for color images. At this stage, each ACA region is represented by a $n \times n$ grayscale image. To extract HOG features, the gradient of each pixel in the region is computed, and then the gradient magnitude is inserted into one of nine histogram bins that span a 180 degree range. The ACA region is divided into $d \times d$ cells, and 2×2 cells form a block. Each block half overlaps each of its neighbors, and is normalized using the L2-norm. With a specific d, the HOG vector is composed of all normalized block histograms. Multiscale strategy is introduced to boost up the performance, *i.e.*, different values of d are used to extract HOG features at different scales, and the final feature is composed of all HOG vectors extracted at every scale. For more details of the HOG features, the readers are referred to [14].

2) Linear SVM classification: For efficiency, a simple linear SVM classifier is employed, with a weight vector ω trained to estimate the class label y (+1 for AC and -1 for OA) of a given feature vector $\mathbf{f}$, according to $y = \omega^T \mathbf{f}$. In the experiments, we use the LIBLINEAR toolbox [16] to train the SVM models.

III. Experiments

In this section, we describe the evaluation criteria and experimental setting, then analyze the classification accuracy in our framework, through comparisons of using visual features and clinical features.

A. Experimental setup

Our approach is implemented with Matlab and tested on a four-core 3.4GHz PC with 12GB RAM. A dataset comprised of 2048 images is used for the experiments, which is much larger than the datasets used in the literature [9][13]. The images are from 8 circular scan videos of 8 patient eyes with glaucoma, 4 of them with PACG and other 4 with POAG. Each video contains 128 frames, and each frame is split into 2 images since it contains two angles and the right angle image is flipped horizontally. The evaluation is based on each single image, which is labeled as AC or OA by three

TABLE I

PERFORMANCE COMPARISONS OF ACA CLASSIFICATION WITH DIFFERENT FEATURES AND PARAMETERS

Feature	HOG				AOD	SLBA
d	3	6	10	{3,6,10}	–	–
AUC	0.807 ±0.073	0.818 ±0.088	0.796 ±0.094	**0.835 ±0.068**	0.745 ±0.166	0.697 ±0.108
$\bar{P}(\%)$	66.8 ±10.0	72.3 ±10.0	67.8 ±7.8	**75.8 ±6.4**	63.9 ±11.7	62.1 ±7.5

ophthalmologists from Singapore Eye Research Institute. All ACA localization results are manually checked and all ACA regions are correctly cropped out. For the ACA classification evaluation, we follow the widely used leave-one-out (LOO) approach, *i.e.*, for each testing round, 512 images from one PACG and one POAG patients are used for testing while others are used for training, thus 16 rounds are performed to test all cases. We assess the performance using a balanced accuracy with a fixed 85% specificity and area under ROC curve (AUC) *which evaluates the overall performance*. The balanced accuracy ($\bar{P}$), sensitivity (P_+) and specificity (P_-) are defined as

$$\bar{P} = \frac{P_+ + P_-}{2}, \quad P_+ = \frac{TP}{TP + FN}, \quad P_- = \frac{TN}{TN + FP}, \tag{1}$$

where TP and TN denote the number of true positives and negatives, respectively, and FP and FN denote the number of false positives and negatives, respectively.

B. Comparison of ACA classification

In this section, we compare classification methods using HOG features [14] with different cell numbers ($d = 3, 6, 10$) and two clinical features (*i.e.*, AOD [10] and SLBA [13]). From the results shown in Table I, we have the following observations:

1) The HOG feature based methods outperform the clinical feature based ones, which demonstrate high dimensional visual features provide more information for classification and thus lead to higher performance. In addition, the performance drops significantly in some videos because the video contains a lot of intermediate cases which are difficult to classify even for human experts.
2) Among methods based on the HOG features with different parameter d, the highest accuracy (*i.e.*, largest AUC and $\bar{P}$) is obtained when setting $d = 6$, for which the cell size is not too small to lose useful information nor too big to introduce more noises.
3) Comparing HOG feature based methods with and without a multiscale scheme, it shows that the multiscale scheme leads to a higher accuracy, as expected.

In terms of processing speed, each ACA costs about 0.09s for feature extraction and classification with a Matlab implementation, which can be further accelerated with a C++ implementation.

IV. CONCLUSION

To identify glaucoma subtype, an image processing and learning based framework was proposed to localize and classify ACA, based on multiscale HOG features. Our method was tested on a clinical dataset comprised of 2048 images with two evaluation criteria. The results indicate that it outperforms clinical feature based methods. In future work, we plan to extend the classification framework to multiple level angle closure grading, in order to elevate precision and better deal with intermediate cases.

REFERENCES

[1] B. Thylefors, A.D. Negrel, R. Pararajasegaram, and K.Y. Dadzie. Global data on blindness, *Bull WHO*, vol. 73, no. 1, pp. 115–21, 1995.

[2] T.Y. Wong, S. Loon, and S.M. Saw. The epidemiology of age related eye diseases in asia, *British Journal of Ophthalmology*, vol. 90, no. 4, pp. 506–11, 2006.

[3] P.J. Foster and G.J. Johnson. Glaucoma in China: how big is the problem? *British Journal of Ophthalmology*, vol. 85, pp. 1277–82, 2001.

[4] B.E. Klein, R. Klein, W.E. Sponsel, T. Franke, L.B. Cantor, J. Martone, and M.J. Menage. Prevalence of glaucoma. The Beaver Dam Eye Study. *Ophthalmology*, vol. 99, pp. 1499–504, 992.

[5] D.T.L. Quek, M.E. Nongpiur, S.A. Perera, and T. Aung. Angle imaging: Advances and challenges, *Indian Journal of Ophthalmology*, vol. 59, no. 7, pp. 69–75, 2011.

[6] N.G. Congdon, Q. Youlin, H. Quigley, P.T. Hung, T.H. Wang, T.C. Ho, and J.M. Tielsch. Biometry and primary angle-closure glaucoma among Chinese, white, and black populations. *Ophthalmology*, vol. 104, pp. 1489–95, 1997.

[7] N.L. Wang, H.P. Wu, and Z.G. Fan. Primary angle closure glaucoma in Chinese and Western populations, *Chinese Medical Journal*, vol. 115, pp. 1706–15, 2002.

[8] J. Cheng, D. Tao., J. Liu, D.W.K. Wong, B.H. Lee, M. Baskaran, T.Y. Wong, and T. Aung. Focal biologically inspired feature for glaucoma type classification, In *Int. Conf. Medical Image Computing and Computer Assisted Intervention*, 2011, vol. 6893, pp. 91–8.

[9] C.K. Leung, W.H. Yung, C.K. Yiu, S.W. Lam, D.Y. Leung, R.K. Tse, C.C. Tham, W.M. Chan, and D.S. Lam. Novel approach for anterior chamber angle analysis: anterior chamber angle detection with edge measurement and identification algorithm (ACADEMIA), *Arch Ophthalmol*, vol. 124, no. 10, pp. 1395–401, 2006.

[10] J. Tian, P. Marziliano, M. Baskaran, H.T. Wong, and T. Aung. Automatic anterior chamber angle assessment for HD-OCT images, *IEEE Trans. on Bio. Eng.*, vol. 58, no. 11, pp. 3242–9, 2011.

[11] C.K. Leung, C.Y. Cheung, H. Li, S. Dorairaj, C.K. Yiu, A.L. Wong, J. Liebmann, R. Ritch, R.N. Weinreb, and D.S. Lam. Dynamic analysis of darkLight changes of the anterior chamber angle with anterior segment OCT, *Invest. Ophthalmol. Vis. Sci.*, vol. 48, no. 9, pp. 4116–22, 2007.

[12] C.K. Leung, H. Li, R.N. Weinreb, J. Liu, C.Y. Cheung, R.Y. Lai, C.P. Pang, and D.S. Lam. Anterior chamber angle measurement with anterior segment optical coherence tomography: a comparison between slit lamp OCT and visante OCT, *Invest. Ophthalmol. Vis. Sci.*, vol. 49, no. 8, pp. 3469–74, 2008.

[13] J. Tian, P. Marziliano, and H.T. Wong. Automatic detection of Schwalbe's line in the anterior chamber angle of the eye using HD-OCT images, In *Int. Conf. IEEE Engin. in Med. and Biol. Soc.*, 2010, pp. 3013–6.

[14] N. Dalal and B. Triggs. Histograms of oriented gradients for human detection, In *IEEE Conf. Computer Vision and Pattern Recognition*, 2005, vol. 1, pp. 1886–93.

[15] Y. Xu., D. Xu, S. Lin, J. Liu, J. Cheng, C.Y. Cheung, T. Aung, and T.Y. Wong. Sliding window and regression based cup detection in digital fundus images for glaucoma diagnosis, In *Int. Conf. Medical Image Computing and Computer Assisted Intervention*, 2011, vol. 6893, pp. 1–8.

[16] R.E. Fan, K.W. Cheng, C.J. Hsieh, X.R. Wang, and C.J. Lin. LIBLINEAR: A library for large linear classification, *Journal of Machine Learning Research*, vol. 9, pp. 1871–4, 2008.